



## Research paper

# Nitro-fatty acids protect against steatosis and fibrosis during development of nonalcoholic fatty liver disease in mice



Oren Rom<sup>a</sup>, Guan Xu<sup>b</sup>, Yanhong Guo<sup>a</sup>, Yunhao Zhu<sup>b</sup>, Huilun Wang<sup>a</sup>, Jifeng Zhang<sup>a</sup>, Yanbo Fan<sup>a</sup>, Wenying Liang<sup>a</sup>, Haocheng Lu<sup>a</sup>, Yuhao Liu<sup>a</sup>, Michael Aviram<sup>c</sup>, Zhipeng Liu<sup>d</sup>, Seongho Kim<sup>e</sup>, Wanqing Liu<sup>f</sup>, Xueding Wang<sup>b</sup>, Y. Eugene Chen<sup>a</sup>, Luis Villacorta<sup>a,\*</sup>

<sup>a</sup> Department of Internal Medicine, Michigan Medicine, Ann Arbor, MI, USA

<sup>b</sup> Department of Radiology, Michigan Medicine, Ann Arbor, MI, USA

<sup>c</sup> The Lipid Research Laboratory, Rappaport Faculty of Medicine, Technion-Israel Institute of Technology, Haifa, Israel

<sup>d</sup> Department of Medicinal Chemistry and Molecular Pharmacology, College of Pharmacy, Purdue University, West Lafayette, Indiana, USA

<sup>e</sup> Biostatistics Core, Karmanos Cancer Institute, Wayne State University, Detroit, MI, USA

<sup>f</sup> Department of Pharmaceutical Sciences and Pharmacology, Wayne State University, Detroit, MI, USA

## ARTICLE INFO

## Article history:

Received 12 October 2018

Received in revised form 7 February 2019

Accepted 7 February 2019

Available online 13 February 2019

## Keywords:

Nitro-fatty acids

Non-alcoholic fatty liver disease

Non-alcoholic Steatohepatitis

Non-invasive liver imaging, liver fibrosis

## ABSTRACT

**Background:** Nonalcoholic fatty liver disease (NAFLD) and resulting nonalcoholic steatohepatitis (NASH) are reaching global epidemic proportions. Lack of non-invasive diagnostic tools and effective therapies constitute two of the major hurdles for a bona fide treatment and a reversal of NASH progression and/or regression of the disease. Nitro-oleic acid (OA-NO<sub>2</sub>) has been proven effective in multiple experimental models of inflammation and fibrosis. Thus, the potential benefit of in vivo administration of OA-NO<sub>2</sub> to treat advanced NAFLD was tested herein in a model of long-term NASH diet-induced liver damage.

**Methods:** Non-invasive imaging (e.g. photoacoustic-ultrasound (PA-US)) was pursued to establish advanced experimental model of NASH in mice in which both steatosis and fibrosis were diagnosed prior experimental therapy with OA-NO<sub>2</sub>. Experimental controls included equimolar amounts of the non-nitrated oleic acid (OA). CLAMS and NMR-based analysis was used for energy metabolism.

**Findings:** CLAMS and NMR-based analysis demonstrates that OA-NO<sub>2</sub> improves body composition and energy metabolism and inhibits hepatic triglyceride (TG) accumulation. Photoacoustic-ultrasound imaging revealed a robust inhibition of liver steatosis and fibrosis by OA-NO<sub>2</sub>. RNA-sequencing analysis uncovered inflammation and fibrosis as major pathways suppressed by OA-NO<sub>2</sub> administration, as well as regulation of lipogenesis and lipolysis pathways, with a robust inhibition of SREBP1 proteolytic activation and subsequent lipogenesis gene expression by OA-NO<sub>2</sub>. These results were further supported by histological analysis and quantification of lipid accumulation, lobular inflammation (F4/80 staining) and fibrosis (collagen deposition, αSMA staining) as well as established parameters of liver damage (ALT). In vitro studies indicate that OA-NO<sub>2</sub> inhibits TG biosynthesis and accumulation in hepatocytes and inhibits fibrogenesis in human stellate cells.

**Interpretation:** OA-NO<sub>2</sub> improve steatohepatitis and fibrosis and may constitute an effective therapeutic approach against advanced NAFLD that warrants further clinical evaluation.

© 2019 Published by Elsevier B.V. This is an open access article under the CC BY-NC-ND license (<http://creativecommons.org/licenses/by-nc-nd/4.0/>).

## 1. Introduction

Nonalcoholic fatty liver disease (NAFLD) is a spectrum of liver disorders characterized by hepatic fat accumulation, inflammation, and

hepatocyte injury [1,2]. In concert with the increased prevalence of obesity due to excess caloric intake and a sedentary lifestyle, the prevalence of NAFLD is increasing worldwide, affecting an estimated 24% of the population [3,4]. NAFLD is associated with increased mortality related to cardiovascular disease (CVD), malignancy and liver disease [3,5]. In up to 40% of individuals, hepatic steatosis progresses to nonalcoholic steatohepatitis (NASH), further characterized by inflammatory infiltrate and hepatocyte injury. A subset of patients develops progressive collagen deposition (fibrosis) [6]. To date, no therapies are available for

\* Corresponding author at: Department of Internal Medicine, Michigan Medicine, North Campus Research Complex, Bld 26, Rm 227N, 2800 Plymouth Rd., Ann Arbor, MI 48109, USA.

E-mail address: [luisvill@med.umich.edu](mailto:luisvill@med.umich.edu) (L. Villacorta).

## Research in context

### Evidence before this study

With nonalcoholic fatty liver disease (NAFLD) and resulting nonalcoholic steatohepatitis (NASH) becoming a growing concern and a major health care issue, efficient therapies to date are underdeveloped. Previous progress in preclinical development of nitro-fatty acids as anti-inflammatory lipid mediators have uncovered benefits on experimental models of metabolic and aligned cardiovascular diseases. However, the therapeutic potential of nitro-fatty acids against NAFLD has not been investigated.

### Added value of this study

This study demonstrates that nitro-oleic acid (OA-NO<sub>2</sub>), a prototypical component of the nitro-fatty acids, is protective against NAFLD in two independent experimental settings: 1) western diet-induced progressive steatosis (apoE knockout mice) and 2) established NASH by long-term administration of high-cholesterol, high fructose diet in wild-type mice (NASH model). A non-invasive imaging approach applied to a NASH model of liver steatosis and fibrosis was further pursued with two aims: 1) to mimic an ideal scenario for NASH diagnosis (avoiding liver biopsy); and 2) to evaluate the putative therapeutic benefits of nitro-fatty acids against established NASH. This study demonstrates that OA-NO<sub>2</sub> reduces clinically-relevant markers of liver damage, and protects against lipid accumulation, lobular inflammation and fibrosis aligned with an overall improvement of metabolism. Both in vivo and in vitro studies demonstrate that OA-NO<sub>2</sub> inhibits triglyceride biosynthesis and accumulation in hepatocytes while inhibiting profibrotic activation of human stellate cells and reducing collagen deposition in the liver.

### Implications of all the available evidence

Current progress in preclinical development of OA-NO<sub>2</sub> has translated into clinical therapeutics in ongoing phase II clinical trials. Yet, our findings expand current knowledge and uncovers OA-NO<sub>2</sub> as readily viable candidates for therapy against NAFLD. While some ongoing trials include obese patients that may provide translational validation of the putative therapeutic benefits of OA-NO<sub>2</sub> against NAFLD, clinical trials specifically designed to test the therapeutic value of OA-NO<sub>2</sub> derivatives for NASH will be critical to pursue.

NASH [6]. Thus identification of novel therapeutic targets against hepatic steatosis, liver inflammation and fibrosis is a major clinical need [7].

Nitroalkene derivatives of unsaturated fatty acids (NO<sub>2</sub>-FAs) have emerged as potent anti-inflammatory and anti-fibrotic signaling mediators [8,9]. NO<sub>2</sub>-FAs are generated during inflammation and digestion through non-enzymatic reactions of unsaturated fatty acids with nitrogen dioxide (:NO<sub>2</sub>), yielding an array of electrophilic NO<sub>2</sub>-FAs with unique biochemical and signaling properties [10,11]. Nitro-oleic acid (OA-NO<sub>2</sub>), exerts protective roles in numerous experimental models of inflammation, imbalanced lipid metabolism and fibrosis [9]. These include endotoxin-induced vascular inflammation and multi-organ injury [12,13], colitis [14], atherosclerosis [15], systemic and pulmonary arterial hypertension (PAH) [16,17], atrial fibrillation and myocardial fibrosis [18,19]. The safety and pharmacokinetics of OA-NO<sub>2</sub> have been clinically examined in four successfully completed phase I trials (NCT02127190, NCT02248051, NCT02460146, NCT02313064) and its

therapeutic potential currently evaluated in phase II clinical trials for the treatment of focal segmental glomerulosclerosis (FSGS), PAH and asthma [9].

Considering the unique pathogenesis of NAFLD involving imbalanced hepatic lipid metabolism, inflammation and fibrosis [1,2] along with the well-established anti-inflammatory and anti-fibrotic properties of OA-NO<sub>2</sub> [7–17] it is plausible to suggest that OA-NO<sub>2</sub> will have a protective effect against NAFLD. Herein, we provide evidence for the protective role of OA-NO<sub>2</sub> against NASH, using non-invasive imaging for NASH diagnosis coupled with histological, molecular and biochemical approaches. Thus, our study provides functional evidence to uncover the putative therapeutic assessment of OA-NO<sub>2</sub> in steatohepatitis and fibrosis.

## 2. Materials and methods

### 2.1. Animal procedures

Eight weeks-old male C57BL/6J (RRID: IMSR\_JAX:000664) and apoE<sup>-/-</sup> (RRID: IMSR\_JAX:002052) mice were fed standard chow diet (CD), Western-diet (WD, Supplementary Tables 1 and 2) or NASH-diet rich in saturated fat, trans-fat, fructose and cholesterol (Supplementary Tables 3 and 4) for 24 weeks. OA-NO<sub>2</sub> was administered via osmotic minipump implantation as described in the Supplementary Materials and Methods.

### 2.2. Non-invasive in vivo imaging for dual analysis of hepatic steatosis and fibrosis

Hepatic lipid and collagen contents were quantitatively determined in vivo in a subgroup of mice by photoacoustic imaging using a photoacoustic-ultrasound (PA-US) dual modality system [20] described in the Supplementary Materials and Methods. During the procedure, mice were anesthetized with ketamine (100 mg/kg) and xylazine (10 mg/kg) injection.

### 2.3. Liver steatosis, lobular inflammation and fibrosis scoring

H&E and Sirius red staining were used to score liver steatosis, lobular inflammation and fibrosis as previously described [21] and elaborated in the Supplementary Materials and Methods.

### 2.4. Statistical analysis

Statistical analyses were performed using SPSS 24.0 software (SPSS Inc. IBM). Unless indicated otherwise, values are presented as box-plots and whiskers or means ± SEM of at least three independent observations. The number of animals or experiments used for each study is specified for each figure legend. One-way analysis of variance (ANOVA) followed by Bonferroni post hoc test was used for data analysis. Differences were considered statistically significant at  $p < .05$ .

### 2.5. Sample-size estimation

The number of mice used for the long-term NASH study was determined by sample-size analysis and calculated based on our initial studies with apoE<sup>-/-</sup> mice (Supplementary Fig. 1), using hepatic TG content as the primary endpoint measure. Using WinPepi statistical software, assuming  $\alpha$  error rate of 0.05 and  $\beta$  error rate of 0.20, the number of mice for the NASH study was  $n = 10$  per group.

### 2.6. Blinding

The following measurements were conducted by technicians blinded to the mouse experimental groups: Liver imaging, pathology, CLAMS, body composition analysis, plasma lipids, and plasma cytokines.

## 2.7. RNA-sequencing biorepository

The RNA-sequencing data discussed in this publication have been deposited in NCBI's Gene Expression Omnibus and are accessible through GEO Series accession number GSE126204 [www.ncbi.nlm.nih.gov/geo/query/acc.cgi?acc=GSE126204](http://www.ncbi.nlm.nih.gov/geo/query/acc.cgi?acc=GSE126204)

## 2.8. Ethics statement

All animal procedures were approved by the Institutional Animal Care & Use Committee of the University of Michigan (PRO00006176) and performed in accordance with the institutional guidelines.

## 3. Results

### 3.1. OA-NO<sub>2</sub> protects against liver steatosis and fibrosis during NASH development

The benefits of OA-NO<sub>2</sub> in pathologies related with imbalanced lipid metabolism were originally observed in hyperlipidemic apoE<sup>-/-</sup> mice in which administration of OA-NO<sub>2</sub> during western-diet (WD) feeding reduced atherosclerosis [15]. However, whether OA-NO<sub>2</sub> can attenuate WD-induced lipid accumulation in the liver is unknown. In initial studies, treatment with OA-NO<sub>2</sub>, but not with non-nitrated OA, prevented early steatosis in apoE<sup>-/-</sup> mice (Supplementary Fig. 1a-1c), attenuated WD-induced hepatic overexpression of key lipogenic genes (e.g. SREBF1, SCD1, Supplementary Fig. 1d) and decreased plasma TG without significant effects on plasma TC, LDL or HDL (Supplementary

Fig. 1e-h). To determine the therapeutic use of OA-NO<sub>2</sub> against NASH, we devised an experimental approach intended to model more advanced stages of NAFLD, a realistic scenario characterized by established coexistence of steatosis and fibrosis (Fig. 1a). To monitor NASH progression, a novel imaging technique was used that provides an accurate simultaneous measurement of both hepatic steatosis and fibrosis in a non-invasive manner. C57BL/6 mice were fed with a NASH diet for 12 weeks (Supplemental Table 3 and 4) and liver pathology was evaluated using high resolution physio-chemical analysis (PCA) [22]. A subset of the animals was sacrificed to confirm established liver steatosis and early fibrosis by histology. Liver PCA revealed enhanced fingerprints in optical wavelengths of 1220 nm and 1370 nm, which identify hepatic lipid and collagen content, respectively (Fig. 1b-c). Histological analysis based on H&E and Oil Red O staining confirmed lipid accumulation and hepatocyte ballooning (Supplementary Fig. 2a-b) while Sirius red staining confirmed collagen deposition and early fibrosis (Supplementary Fig. 2c).

After confirmatory concurrence of hepatic steatosis and fibrosis, animals were randomized to receive OA-NO<sub>2</sub>, OA as non-nitrated fatty acid control and PEG, which served as vehicle, via osmotic minipumps implantation for additional 12 weeks under ad libitum NASH-diet feeding (Fig. 1a). Two weeks before terminal analysis, non-invasive photoacoustic ultrasound (PA-US) based-imaging was further pursued in all experimental groups to quantitatively determine whether OA-NO<sub>2</sub> treatment was effective against progressive NASH. Liver pathology evaluated using high resolution PCA revealed a progressively enhanced fingerprints of hepatic lipid content (1220 nm optical wavelength, Fig. 1d) and collagen content (1370 nm optical wavelength, Fig. 1e) in NASH

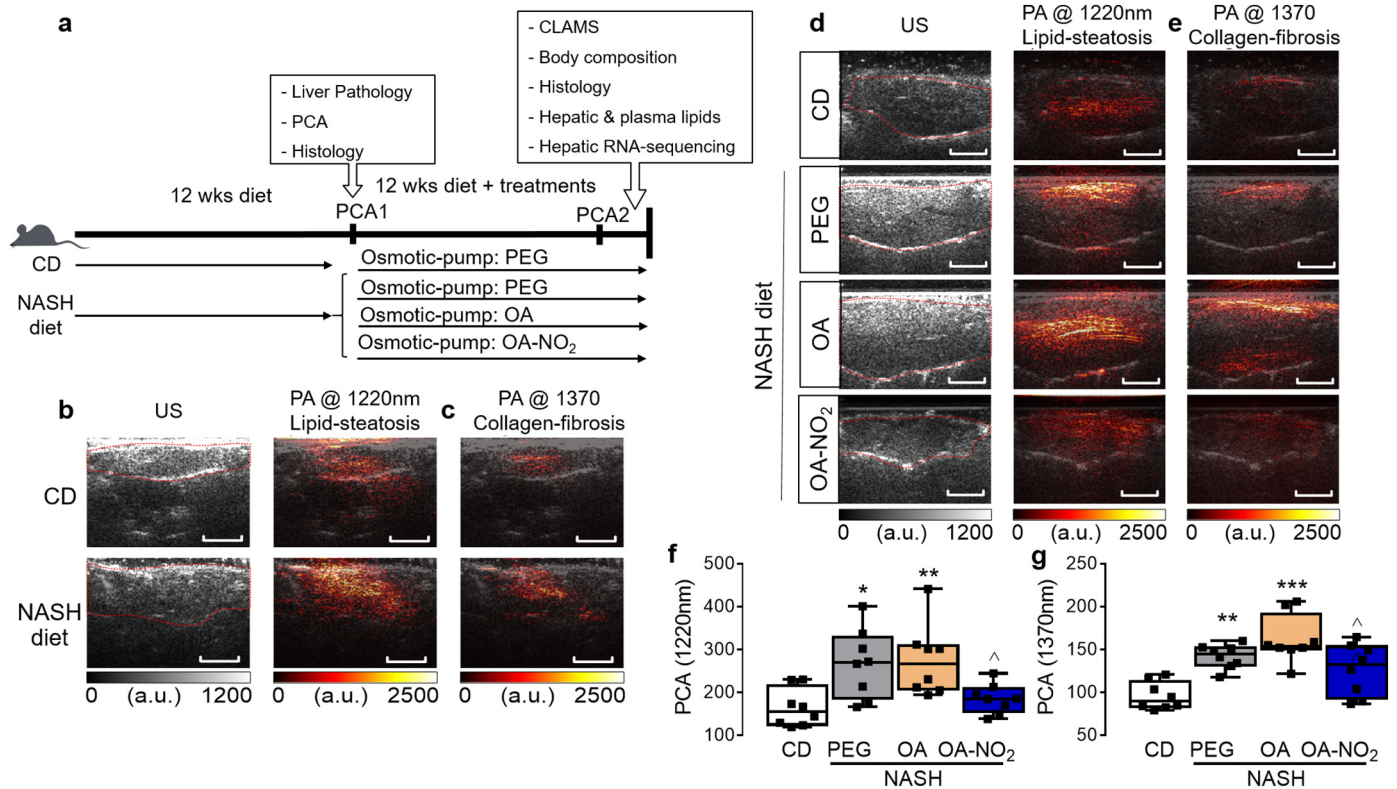


**Fig. 1.** Non-invasive diagnosis reveals OA-NO<sub>2</sub> protection against NASH-diet induced hepatic steatosis and fibrosis. (a) Experimental design: Steatohepatitis was induced in C57BL/6 mice by a NASH diet, rich in saturated fat, trans fat, fructose and cholesterol for 12 weeks. After 12 weeks, high-resolution physio-chemical analysis ultrasound (PCA-US), confirmed coexistence of lipid steatosis and early fibrosis. Then, osmotic minipumps were implanted subcutaneously to deliver PEG, OA or OA-NO<sub>2</sub> (5 mg/kg/d) for additional 12 weeks under chow diet (CD) or NASH-diet feeding (4 groups, n = 10 per group). Established liver damage was confirmed in a subpopulation (n = 3) analyzed after 12 weeks using (b) conventional ultrasound (US) combined with high-resolution PCA high-resolution at 1220 nm optical wavelength to detect hepatic lipids, and (c) at 1370 nm optical wavelength to quantify hepatic collagen content. Two weeks before terminal analysis of liver pathology PA-US was used to quantitatively analyze lipid content and total collagen content in the NASH-diet model. High-resolution PCA demonstrated a marked reduction of total hepatic lipid (d) and collagen content (e) upon OA-NO<sub>2</sub> treatment compared to non-nitrated OA. Quantitative analysis of PA absorption from each experimental group at 1220 nm (f) and 1370 nm fingerprint (g). Size bars = 5 mm Data is plotted as box and whiskers from minimum to maximum values showing all points. \*p < .05, \*\*p < .01, \*\*\*p < .001 vs. CD; ^p < .05, vs. NASH OA. n = 8.

diet-fed mice treated with either PEG or OA compared to CD-fed mice. Treatment with OA-NO<sub>2</sub> markedly suppressed both NASH diet-induced hepatic lipid accumulation and collagen deposition, quantified by the lower magnitude of the PA signals at 1220 nm (Fig. 1f) and 1370 nm (Fig. 1g), respectively.

3.2. OA-NO<sub>2</sub> improves body composition and promotes a metabolic phenotype in NASH-diet fed mice similar to CD feeding

Gross appearance of the peritoneal cavities at the experimental end-point (24 weeks) revealed substantial hepatic steatosis with enlarged visceral fat pads in NASH-diet fed mice administrated with PEG or OA, which were attenuated by OA-NO<sub>2</sub> (Fig. 2a). Body-weight measurement, showed a trend towards reduced body weight gain upon OA-NO<sub>2</sub> administration, reaching statistical significance compared with NASH PEG group but not with OA (*p* < .05, Supplementary Fig. 3a). Yet, NMR-based analysis of body composition indicated that body fat was significantly reduced by OA-NO<sub>2</sub> along with a significant increase in lean body mass (Fig. 2b-c).

The metabolic response to obesity involves a shift towards greater lipid versus lower carbohydrate utilization, reflecting a reduction in respiratory quotient (respiratory exchange ratio-RER) [23,24]. Accordingly, CLAMS analysis indicated a pronounced reduction of RER in response to NASH-diet, both in the OA or PEG vehicle-treated controls (Fig. 2d-e), reflecting an increased fat oxidation (Supplementary Fig. 4a), and decreased glucose oxidation (Supplementary Fig. 4b) in these experimental groups. OA-NO<sub>2</sub> treatment, however, partially reversed this trend towards a reduced fat oxidation and increased glucose oxidation, resulting in a significant elevation of the respiratory quotient (Fig. 2d-e). No significant differences in energy expenditure, or

ambulatory activity (Supplementary Fig. 4c-d) were observed between the groups.

3.3. OA-NO<sub>2</sub> protects against steatohepatitis, hepatomegaly and liver damage in NASH

Chronic NASH-diet feeding for a total of 24 weeks resulted in a significant increase in body weight irrespectively of intervention with PEG or OA (*p* < .001 or *p* < .05, respectively) compared to CD, with a similar trend in mice treated with OA-NO<sub>2</sub> (*p* = .113, Supplementary fig. 3a). Livers were drastically enlarged in the PEG- and OA-treated group (3.28 ± 0.12 g, 3.06 ± 0.14, respectively, *p* < .001, Fig. 3a and Supplementary Fig. 3b) but not in the OA-NO<sub>2</sub> group, which exhibited significantly reduced liver to body weight ratios (Fig. 3b).

Histological analysis based on H&E staining and NAFLD activity scoring, indicated that PEG control and OA-treated groups exhibited histologic features characteristic of NASH, including micro- and macrovesicular steatosis, hepatocyte ballooning, and infiltration of inflammatory cells. Notably, following OA-NO<sub>2</sub> administration, steatosis and inflammation scores were significantly decreased, while hepatocyte ballooning remained unaltered compared to PEG or OA (Table 1). Oil red O staining was significantly reduced in the OA-NO<sub>2</sub> group (Fig. 3a). Furthermore, OA-NO<sub>2</sub> markedly reduced systemic markers of liver damage, ALT and AST (Fig. 3c-d), as well as hepatic TG mass (Fig. 3e) but not liver cholesterol (Fig. 3f). Overall, NAFLD activity score, defined as the additive score for steatosis, ballooning and inflammation was significantly lower upon treatment with OA-NO<sub>2</sub> compared to PEG control (4.1 ± 0.5 vs. 6.2 ± 0.4, *p* < .001), and a similar trend was noted compared to OA (5.7 ± 0.4, *p* = .063) (Table 1). Accordingly, linear regression analysis indicated a positive and significant correlation between individual

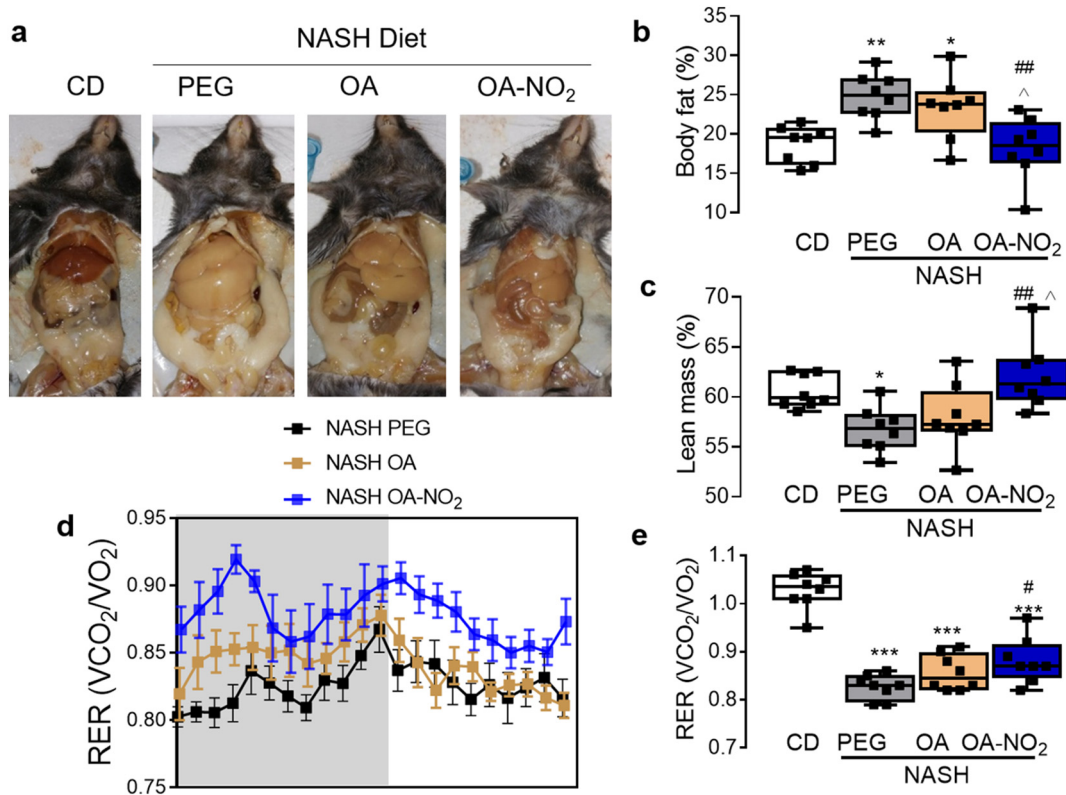


**Fig. 2.** OA-NO<sub>2</sub> improves body composition and increases respiratory quotient in NASH-diet induced steatohepatitis. (a) Gross appearance of the peritoneal cavity at the experimental end-point (24 weeks) depicting apparent reduction of liver steatosis upon treatment with OA-NO<sub>2</sub>. One week before end-point analysis, NMR-based body composition analysis was conducted (n = 8) revealing a significant reduction of % body fat (b) and subsequent increase in % lean body mass (c), upon OA-NO<sub>2</sub> treatment. No alteration in body composition was observed in mice treated with equimolar amounts of non-nitrated OA. Quantitative data is plotted as box and whiskers from minimum to maximum values showing all points. (d) OA-NO<sub>2</sub> increased the respiratory exchange ratio (RER) calculated as the ratio of CO<sub>2</sub> generation vs. oxygen consumption (VCO<sub>2</sub>/VO<sub>2</sub>) assessed by CLAMS. Data are shown over a 24 h dark/light period cycle (n = 8). (e) Quantitative analysis of RER in each experimental group shown as box and whiskers from minimum to maximum values. Data is shown as mean ± SEM. \**p* < .05, \*\**p* < .01, \*\*\**p* < .001 vs CD PEG; \**p* < .05, \*\**p* < .01, \*\*\**p* < .001 vs. NASH PEG; #*p* < .05 vs. NASH OA.

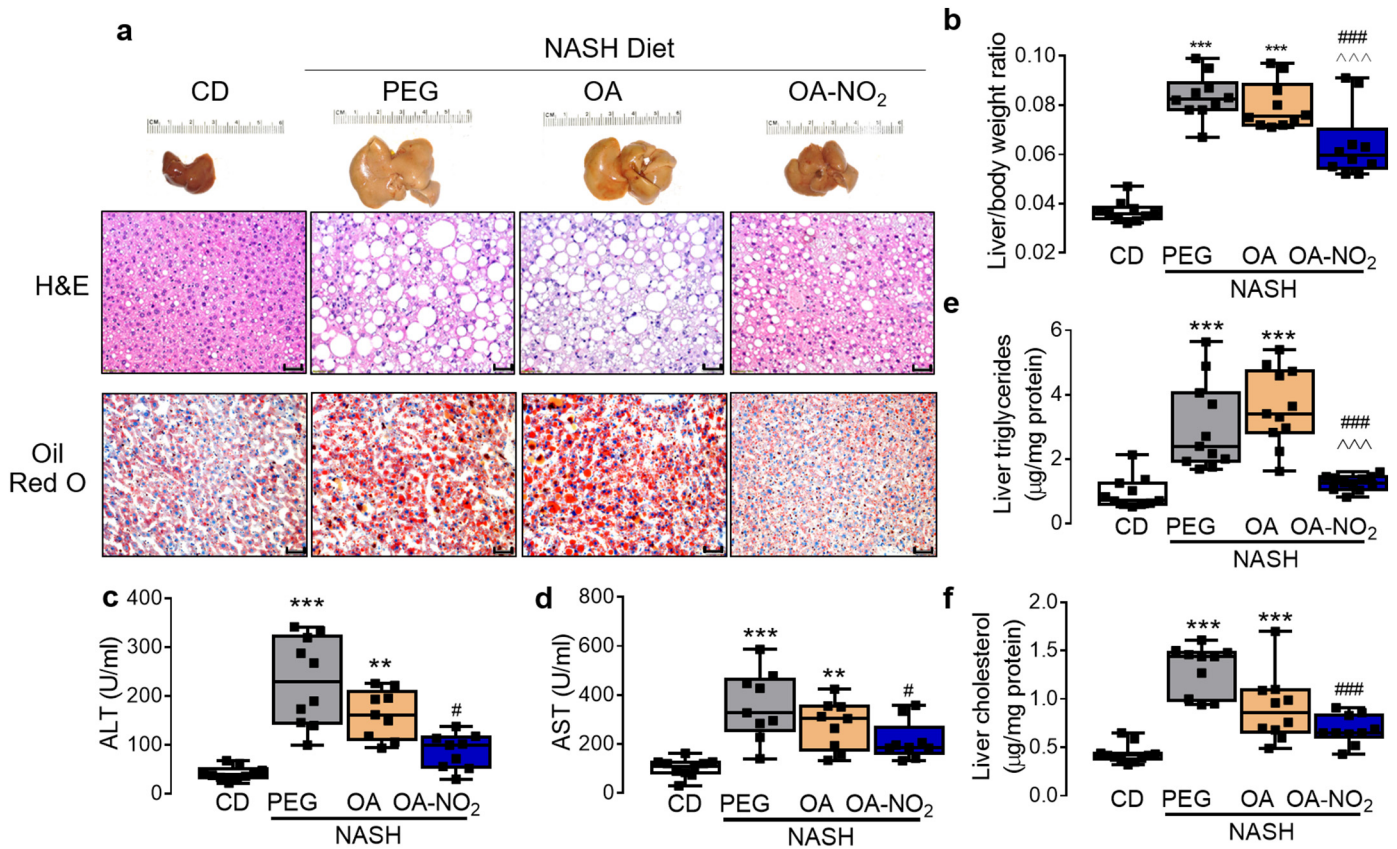


**Fig. 3.** OA-NO<sub>2</sub> prevents NASH diet-induced hepatomegaly and liver damage, and improves NAFLD activity scores. (a) Gross liver morphology, H&E and Oil Red O histology from each experimental group. H&E histology was used for quantitative NAFLD scoring as described and summarized in Table 1. (b) Quantitative analysis of hepatomegaly was determined as of liver to body weight ratio. (c) Fasting plasma analysis of alanine aminotransferase (ALT) and (d), aspartate aminotransferase (AST). (e) Hepatic triglyceride mass and (f) cholesterol mass from each experimental group. Quantitative data is plotted as box and whiskers from minimum to maximum values showing all points. \**p* < .05, \*\**p* < .01, \*\*\**p* < .001 vs CD/PEG; #*p* < .05, ##*p* < .01, ###*p* < .001 vs. NASH PEG ^*p* < .05, ^^*p* < .01, ^^*p* < .001, vs. NASH OA.

NAFLD activity scores and ALT or AST levels and suggest that OA-NO<sub>2</sub> administration improves NASH-diet induced liver damage (Supplementary Fig. 5a). Systemically, OA-NO<sub>2</sub> reduced fasting glucose levels whereas the non-nitrated control OA had no significant effect (Supplementary Fig. 5b). Similarly, fasting plasma lipid profile analysis revealed a normalization of plasma TG levels by OA-NO<sub>2</sub> but not OA (Supplementary Fig. 5c). In contrast, OA-NO<sub>2</sub> had no protective effect against NASH diet-induced hypercholesterolemia (Supplementary Fig. 5d).

### 3.4. OA-NO<sub>2</sub> reverses NASH-diet-induced dysregulation of hepatic genes involved in NASH

Next, an unbiased analysis of hepatic gene expression by RNA sequencing (RNA-seq) was pursued after 12 weeks of PEG, OA and

OA-NO<sub>2</sub> delivery under NASH-fed diet conditions. Principal component analysis (PCA) revealed that the gene expression profile of the NASH-diet fed mice either treated with PEG or OA clustered together resulting in major changes in gene expression compared to CD (Supplementary Fig. 6a). Systemic administration of OA-NO<sub>2</sub> resulted in an intermediate profile between the CD group and the NASH-diet induced changes in gene expression in the liver (Supplementary Fig. 6a). Volcano plot analysis of the differentially expressed genes (DEGs) further revealed global changes in gene expression patterns between NASH diet-fed PEG vs. CD (Fig. 4a) or between OA vs. CD (Fig. 4b). However, DEGs of the OA-NO<sub>2</sub> group substantially differ from those regulated by OA, resulting in a gene expression pattern comparable to CD (Fig. 4c). Venn diagrams further illustrate the similarity of the gene expression profile between NASH-diet with either

**Table 1**  
NAFLD activity score in response to OA-NO<sub>2</sub>.

	Steatosis	Hepatocyte ballooning	Lobular inflammation	NAFLD activity score
CD	0.8 ± 0.2	0.5 ± 0.2	0.2 ± 0.1	1.5 ± 0.4
PEG	2.9 ± 0.1 ***	1.8 ± 0.1 ***	1.5 ± 0.3 **	6.2 ± 0.4 ***
OA	2.6 ± 0.2 ***	1.9 ± 0.1 ***	1.2 ± 0.3 *	5.7 ± 0.4 ***
OA-NO <sub>2</sub>	2.0 ± 0.3 ** #	1.6 ± 0.2 ***	0.5 ± 0.2 #	4.1 ± 0.5 ** ##

NAFLD scoring: from 0 to 3 (0: <5%steatosis; 1: 5–33%; 2: 34–66%; 3: >67%), hepatocyte ballooning from 0 to 2 (0: normal hepatocytes, 1: normal-sized hepatocytes with pale cytoplasm, 2: pale and enlarged hepatocytes, at least 2-fold than normal hepatocytes), lobular inflammation from 0 to 2 based (0: none, 1: <2 foci; 2: ≥2 foci). NAFLD activity score was calculated as the sum of steatosis, hepatocyte ballooning and lobular inflammation scores.

\* *p* < .05

\*\* *p* < .01

\*\*\* *p* < .001 vs. CD.

# *p* < .05.

## *p* < .01 vs. NASH PEG.

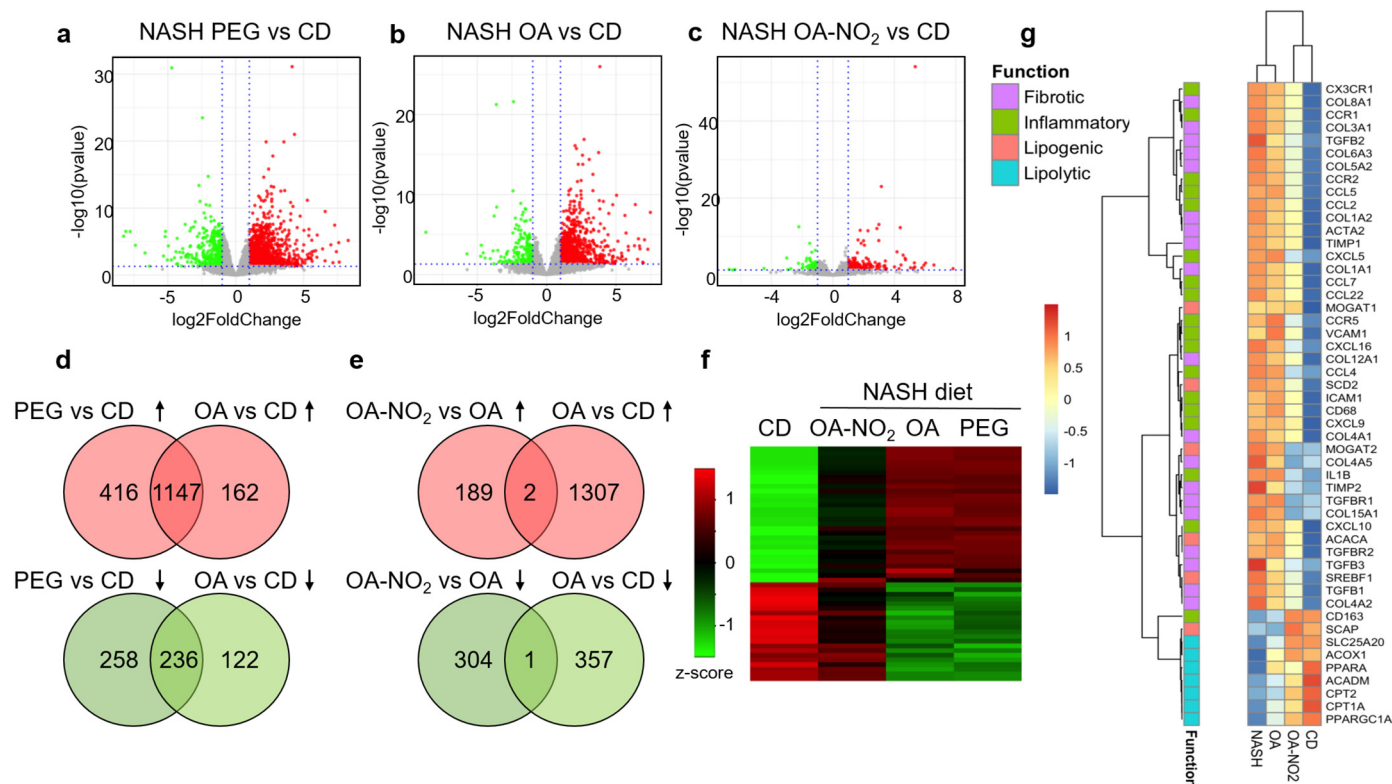


**Fig. 4.** Global hepatic transcriptomic profile in response to OA-NO<sub>2</sub> analyzed by RNA-sequencing. Volcano plots of differentially regulated genes (DEGs) in (a) NASH (PEG) vs. chow diet group (CD); (b) OA vs. CD and (c) OA-NO<sub>2</sub> vs. CD. Principal component analysis (PCA) plot and additional volcano plot comparisons between groups are depicted in Supplementary Fig. 5a and b. X axis represents the log<sub>2</sub>FoldChange of each gene, and Y axis represents the -log<sub>10</sub> transformation of the p values. Genes with p values <.05 and log<sub>2</sub>FoldChange larger than 1 were considered significant DEGs. Up-regulated DEGs are depicted in red, down-regulated DEGs in green, and the non-significant genes in grey. (d) Venn diagrams showing common DEGs in the NASH-diet (PEG) and OA vs. chow diet (CD). (e) Venn diagrams showing DEGs dissimilarity in the OA-NO<sub>2</sub> group vs. OA. (f) Heatmap depicting the top 50 DEGs among all experimental groups as determined by log<sub>2</sub>FoldChange compared with CD group. Each row represents one gene, and each column represents one comparison to CD group. The log<sub>2</sub>FoldChange was row scaled and depicted by colors. (g) Heatmap of 50 NASH-related genes. The classification of the genes based on their function in inflammation, fibrosis, lipogenesis and lipolysis was labeled by different colors as shown at the left side of the heatmap.

PEG or OA treatment, with >1000 shared genes upregulated and > 200 downregulated between those groups (Fig. 4d). In sharp contrast, the gene expression profile from the OA-NO<sub>2</sub> group is almost entirely dissimilar to the non-nitrated OA (Fig. 4e), suggesting that OA-NO<sub>2</sub> induces a distinct hepatic gene expression pattern. Indeed, focusing the analysis on the top DEGs across all experimental groups, heatmap-based representation shows a distinct separation in gene expression patterns in the OA-NO<sub>2</sub> group compared to PEG or OA (Fig. 4f). Pathway enrichment analysis comparing OA-NO<sub>2</sub> with the non-nitrated OA, revealed a significant down-regulation of key pathways involved in enhanced inflammation in NASH by OA-NO<sub>2</sub> (TREM signaling, NF-κB signaling, chemokine signaling, inflammasome pathway, TLR signaling), and hepatic fibrosis, hepatic stellate cell activation and atherosclerosis signaling (Supplementary fig. 7a). In contrast, key pathways involved in fatty acid utilization (fatty acid β-oxidation or mitochondrial L-carnitine shuttling) were enriched by OA-NO<sub>2</sub> compared to OA administration (Supplementary Fig. 7b). Analysis of 50 genes related to key steps of NASH development and progression (Fig. 4g), revealed that OA-NO<sub>2</sub> suppressed NASH-diet-induced lipogenic gene expression (SREBF1, MOGAT2, SCD2) while inducing lipolysis (CPT1A, CPT2, PPARGC1A). Notably, treatment with OA-NO<sub>2</sub>, but not OA, attenuated NASH-diet-induced upregulation of key pro-inflammatory genes (ICAM-1, IL1B, CCL2, CCL5, CCR2, CX3CR1) and pro-fibrotic genes (TGFB1, TGFB2 and TGFB3, TGFB1, TGFB2, COL1A2, ACTA2, TIMP1, TIMP2). Taking together, an unbiased analysis of hepatic gene expression revealed that treatment with OA-NO<sub>2</sub> during NASH reverses impaired lipid

metabolism, enhanced inflammation and fibrosis, main pathophysiological pathways of NASH progression.

### 3.5. OA-NO<sub>2</sub> protects against hepatic steatosis by normalizing NASH diet-impaired lipid metabolism

Validation of DEGs using qPCR analysis indicated that de novo lipogenesis genes were strongly induced in response to NASH-diet feeding, and reduced by OA-NO<sub>2</sub> (Fig. 5a). These include sterol regulatory element binding protein-1 (SREBP-1)-dependent gene expression, including stearoyl-CoA desaturase (SCD1) and glycerol-3-phosphate O-acyltransferase2 (GPAT2). In contrast, genes involved in fatty acid β-oxidation including CPT2, HSD17B10, ACSL1 and PPARGC1A were markedly down-regulated by NASH-diet feeding, but not in the OA-NO<sub>2</sub> group (Supplementary Fig. 8). Western blot analysis revealed that SREBP1 expression as well as its maturation were induced in response to NASH-diet feeding, and reduced by OA-NO<sub>2</sub> (Fig. 5b). Studies in primary hepatocytes and HepG2 cells in response to lipid overload (Fig. 5c-d) or [<sup>3</sup>H]-acetate incorporation into TG (Fig. 5e), indicated that OA-NO<sub>2</sub> inhibits TG biosynthesis and accumulation, whereas OA has modest effects. The above results highlight the protective effects of OA-NO<sub>2</sub> against NASH diet-induced hepatic steatosis attributed to its effects on normalizing expression of genes regulating de novo lipogenesis, inhibiting SREBP1 maturation and in accordance, preventing TG biosynthesis and accumulation in the liver.

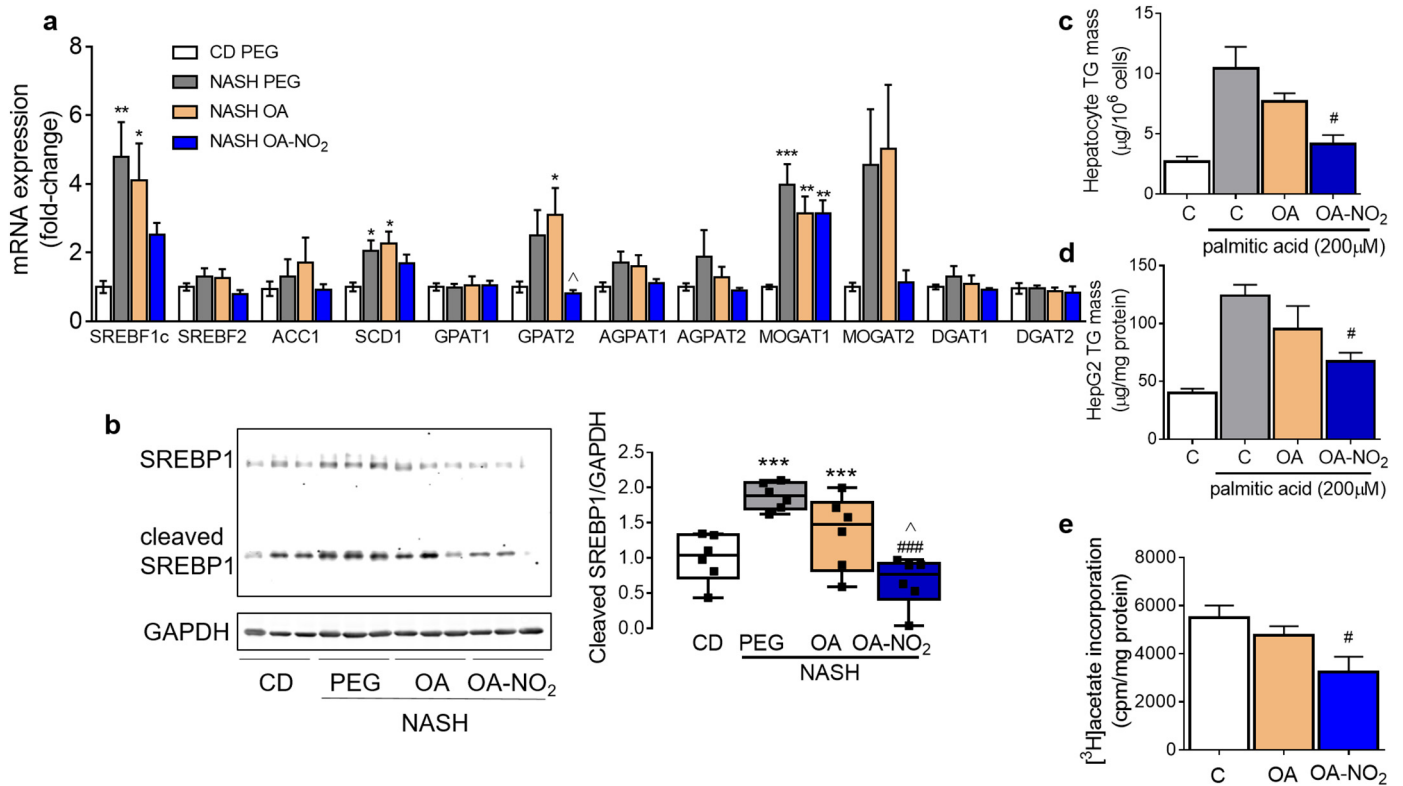


**Fig. 5.** OA-NO<sub>2</sub> inhibits hepatocyte triglyceride accumulation. (a) qPCR analyses of hepatic expression of genes regulating lipid biosynthesis. Data presented in bars are means  $\pm$  SEM ( $n = 7-10$ ). (b) Total liver lysates from each experimental group were subjected to western blot analysis of precursor, cleaved SREBP1 and GAPDH as loading control. Quantitative densitometry analysis is shown as box and whiskers from minimum to maximum values showing all points ( $n = 6$ ). \* $p < .05$ , \*\* $p < .01$ , \*\*\* $p < .001$  vs CD PEG; ### $p < .001$  vs. NASH PEG ^ $p < .05$  vs. NASH OA. (c) Triglyceride (TG) content in primary hepatocytes and HepG2 cells treated with or without palmitic acid (200  $\mu$ M), OA or OA-NO<sub>2</sub> (1  $\mu$ M) for 20 h. # $p < .05$  vs. palmitic acid ( $n = 3$ ). (b) TG biosynthetic rate determined using [<sup>3</sup>H]-acetate incorporation into TG in HepG2 cells treated with either OA or OA-NO<sub>2</sub> (1  $\mu$ M) for 6 h ( $n = 3$ ). # $p < .05$  vs. vehicle control (EtOH).

### 3.6. OA-NO<sub>2</sub> reduces NASH diet-induced hepatic and systemic inflammation

In addition to lipid metabolism, pathway analysis also identified relevant processes involved in inflammation and immune cellular response including TREM, NF $\kappa$ B or TLR signaling, leukocyte extravasation, or nitric oxide production in macrophages (Supplementary Fig. 7a). Indeed, hepatic inflammation was significantly reduced by OA-NO<sub>2</sub> as revealed by immunostaining for F4/80, a well-established histological marker of macrophage infiltration (Fig. 6a). Inflammatory gene expression was induced by NASH-diet feeding and reduced by OA-NO<sub>2</sub> treatment. These include intercellular adhesion molecule-1 (ICAM-1), triggering receptor expressed on myeloid cells 2 (TREM2) and toll like receptors (TLR1, 2 and 4) (Fig. 6b). Proinflammatory cytokine expression in the liver, including tumor necrosis factor- $\alpha$  (TNF $\alpha$ ), interleukin-1 $\beta$  (IL-1 $\beta$ ), C—C motif chemokine ligand 2 (CCL2) and CCL5, was significantly reduced upon OA-NO<sub>2</sub> treatment (Fig. 6c). Moreover, markers of systemic inflammation were reduced by OA-NO<sub>2</sub> as evident by reduced levels of plasma MCP-1 and IL-6 (Fig. 6d–e).

### 3.7. OA-NO<sub>2</sub> protects against NASH-induced hepatic fibrosis

Since photoacoustic ultrasound analysis identified a significant reduction of hepatic collagen content in response to OA-NO<sub>2</sub> treatment (Fig. 1), the effect of OA-NO<sub>2</sub> on hepatic fibrogenesis was further examined. Histological analysis based on Sirius red staining,  $\alpha$ -smooth muscle actin ( $\alpha$ SMA) immunohistochemistry (Fig. 7a), and fibrosis scoring revealed a protective role of OA-NO<sub>2</sub> against NASH-diet-induced liver fibrosis, whereas OA administration was ineffective (Table 2). Hepatic collagen content (hydroxyproline) end-point analysis revealed a

significant reduction of hepatic fibrosis upon OA-NO<sub>2</sub> administration (Fig. 7b). RNA-sequencing analysis identified pro-fibrotic pathways activated in NASH, primarily hepatic fibrosis and stellate cell activation particularly related to activation of TGF $\beta$  signaling (Fig. 4f and Supplementary Fig. 7). Thus, we next analyzed whether OA-NO<sub>2</sub> administration reduces TGF $\beta$ -mediated hepatic fibrosis (e.g. SMAD signaling). Indeed, quantitative analysis of NASH-induced SMAD2 activation (e.g. phosphorylated-SMAD vs. total SMAD) was significantly blunted by OA-NO<sub>2</sub> (Fig. 7c). Furthermore, fibrogenic gene expression, including connective tissue growth factor (CTGF), collagen type 1 alpha 2 chain (Col1a2), tissue inhibitor of metalloproteinases1 (TIMP1), and ACTA2 was markedly reduced upon OA-NO<sub>2</sub> treatment (Fig. 7d). In human stellate cells (HSCs), OA-NO<sub>2</sub> inhibited TGF $\beta$ -induced CTGF and  $\alpha$ SMA protein expression in a dose-dependent manner (Fig. 7e) and inhibited profibrotic TGF $\beta$ -dependent activation of human stellate cells. mRNA expression of ACTA2, CTGF, Col1a1, and Col1a2 was significantly reduced by OA-NO<sub>2</sub> upon activation by TGF $\beta$ , whereas OA had no effect (Fig. 7f).

## 4. Discussion

NASH is emerging as one of the major public health issues in the 21st century due to an ever increasing overnutrition aligned with a more prevalent sedentary lifestyle. While NAFLD and resulting NASH are reaching global epidemic proportions, clear diagnosis, primarily limited to liver biopsy, and lack of approved drugs constitute two of the major hurdles of an effective treatment. Thus, advances in non-invasive diagnostic tools and effective antifibrotic therapies are paramount for reversing NASH progression and/or regression of the disease [25]. The present study used a non-invasive imaging approach applied to a NASH model of liver steatosis and fibrosis to evaluate the putative therapeutic benefits of OA-NO<sub>2</sub> against NASH. Our experimental settings

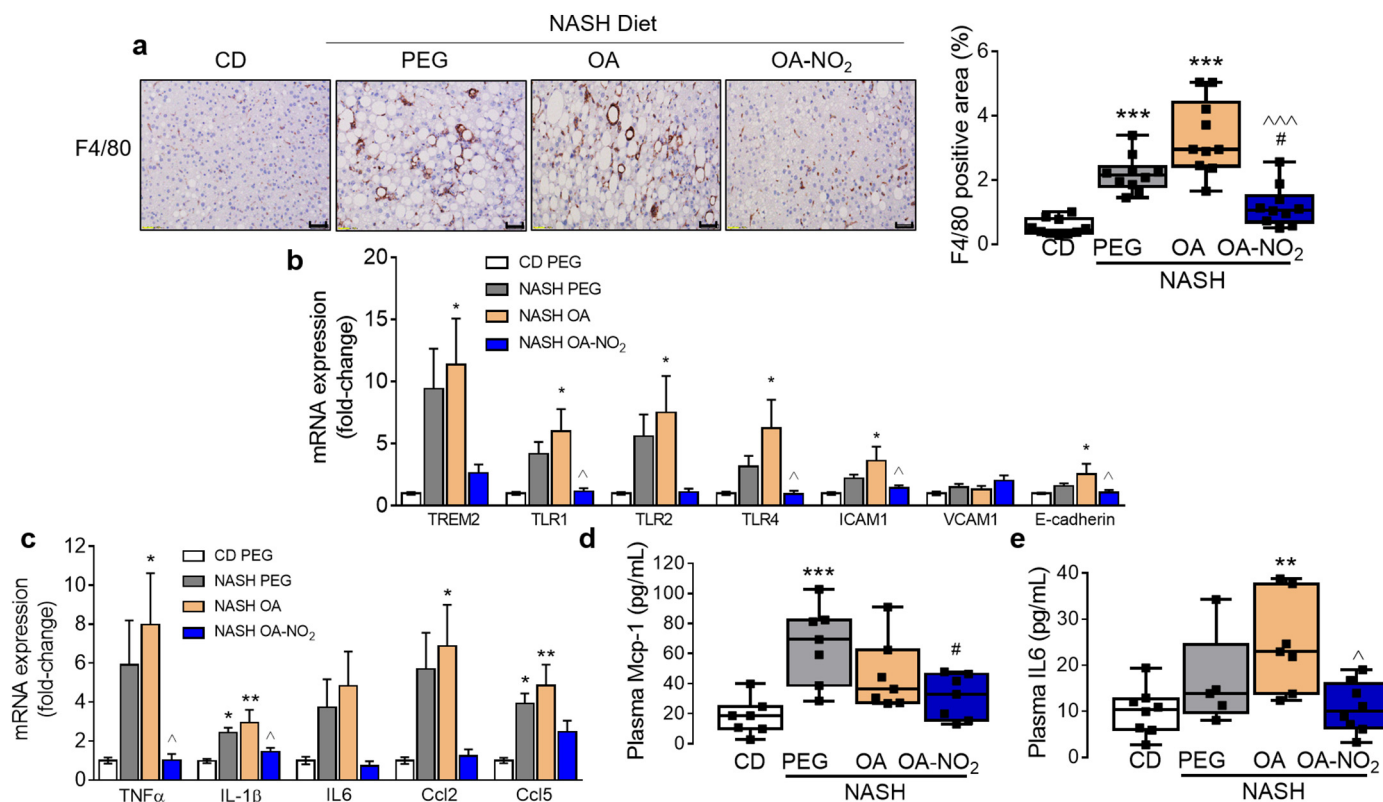


**Fig. 6.** OA-NO<sub>2</sub> inhibits NASH-diet induced hepatic and systemic inflammation. (a) Representative F4/80 immunohistochemistry from each experimental group. Positive areas were calculated using ImageJ to determine F4/80 immunohistochemistry. Scale bar: 50  $\mu$ m. (b) qPCR validation of inflammatory gene expression in the liver including TREM2, TLRs and adhesion molecules ICAM1, VCAM1 and E-cadherin. (c) Common cytokine mRNA expression levels and (d) plasma pro-inflammatory biomarkers Mcp-1 and IL6. Quantitative data is plotted as box and whiskers from minimum to maximum values showing all points. \* $p < .05$ , \*\* $p < .01$ , \*\*\* $p < .001$  vs CD PEG; # $p < .05$ , vs. NASH PEG; ^ $p < .05$ , ^^ $p < .001$  vs. NASH OA.

were specifically designed to address whether OA-NO<sub>2</sub> administration is a valid therapeutic approach at the onset of NASH, requiring conditions in which both steatosis and fibrosis were concurrently established. Therefore, non-invasive imaging approaches were pursued (e.g. photoacoustic imaging), envisioning an ideal diagnostic tool as a valid alternative to liver biopsy thoroughly sought-after in the clinical settings [26]. This imaging modality has the potential to simultaneously monitor lipids and collagen as well as hemoglobin and water content when operating at the full optical spectrum [22]. Herein, the analysis focused on the lipid and collagen components for the purpose of providing a quantitative measurement of their liver content upon OA-NO<sub>2</sub> treatment. This approach provided a useful platform to validate the presence of established hepatic steatosis and fibrosis after 3 months of NASH-diet feeding prior randomization and treatment for an additional 3 months with OA-NO<sub>2</sub>. This scenario thus resembles more advanced experimental models of NASH rather than progressive development of diet-induced NAFLD [22,27]. Herein, we provide evidence of a protective role of OA-NO<sub>2</sub> against NASH. Remarkably, these studies indicate that OA-NO<sub>2</sub> is beneficial against two major hallmarks of advanced NAFLD (e.g. lipid accumulation and fibrosis) [28]. Yet, this current study cannot address whether intervention with OA-NO<sub>2</sub> has the potential to reverse NASH.

Analysis of both hepatic and systemic lipid profile suggest that OA-NO<sub>2</sub> has a significant impact on triglyceride metabolism, with minor effect on cholesterol metabolism. Unbiased analysis of global gene expression and pathway analysis identified inhibition of lipogenesis and enhanced lipolysis in response to OA-NO<sub>2</sub>. OA-NO<sub>2</sub> inhibits NASH-induced SREBP1 maturation and thus ensuing inhibition of lipogenesis by OA-NO<sub>2</sub> and conversely activation of lipolysis. Other possibilities, however, cannot be excluded. For example, diversion of lipid metabolism away from the liver to other peripheral tissues (in particular adipose tissue) is considered a possible therapeutic alternative to

NASH [29]. NO<sub>2</sub>-FAs are broadly distributed throughout the adipose tissue, where they undergo esterification [30]. CLAMS and NMR-based body composition analysis indicate that OA-NO<sub>2</sub> favors a lean versus fat phenotype with only modest effects in body weight, which may also reflect of a favorable metabolism in the adipose tissue.

Regulation of inflammatory responses is a central mechanism by which OA-NO<sub>2</sub> exert beneficial outcomes in various experimental models [31]. Here, a comprehensive analysis of steatosis, inflammation and fibrosis was pursued in response to OA-NO<sub>2</sub> administration. Histological analysis demonstrates that OA-NO<sub>2</sub> improves hepatic steatosis and attenuates lobular inflammation concomitant with a reduction of inflammatory markers, including Kupffer cell/macrophage activation, F4/80, or pro-inflammatory cytokine expression (e.g. TNF $\alpha$ , IL-1 $\beta$ , IL-6, CCL2, and CCL5) as well as reduced plasma levels of IL-6 and MCP-1. Indeed, therapeutic inhibition or resolution of inflammation reduces steatohepatitis and liver fibrosis in NASH models [32]. Specialized pro-resolving lipid mediators (SPM, derived mainly from omega 3 polyunsaturated fatty acids, n-3 PUFAs), exert protective effects on hepatic and adipose tissue with observed benefits in animal models of obesity. However, administration of n-3 PUFAs to NAFLD patients is not effective in improving hepatocyte injury or fibrosis [34]. Our findings indicate that NO<sub>2</sub>-FA, a new class of regulators of inflammation and fibrosis, may be an innovative lipid-based therapeutic strategy against NASH, encouraging subsequent validation in clinical settings [33].

Regarding potential mechanisms operated by OA-NO<sub>2</sub>, we found that OA-NO<sub>2</sub> regulates several pathophysiological processes during NASH progression. These include limiting hepatocyte TG accumulation; attenuation of diet-induced systemic inflammation as well as in the liver; and inhibition of hepatic fibrogenesis. These pathological processes operate in a step-wise manner during NASH and overlap in more advanced stages of the disease [27]. Thus, the protective effect of OA-NO<sub>2</sub> against NASH cannot be ascribed to a single process. Rather,

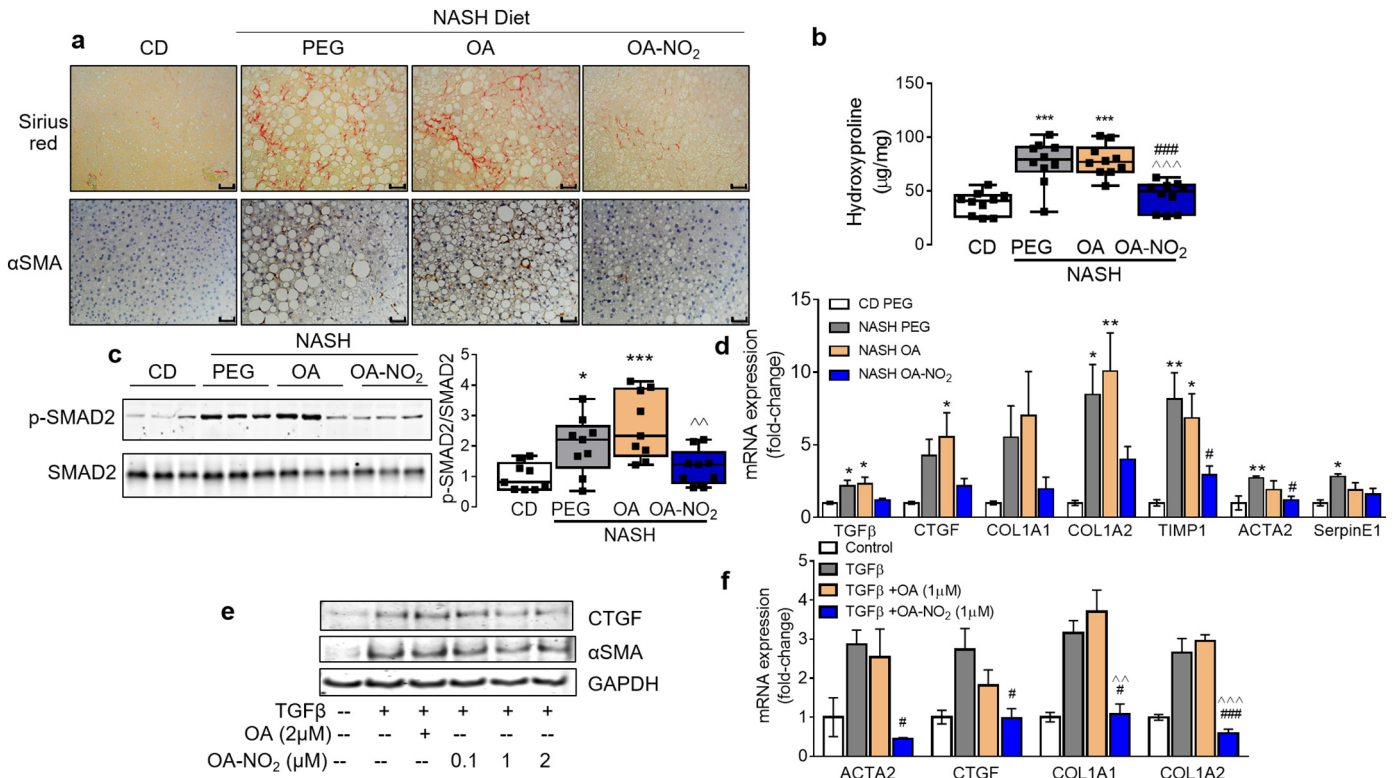


**Fig. 7.** OA-NO<sub>2</sub> regulates hepatic fibrogenic signaling in vivo and in human stellate cells in vitro and inhibits liver fibrosis in NASH. (a) Representative Sirius Red histology and αSMA immunohistochemistry from each experimental group. Scale bar: 50 μm. Positive areas were calculated using ImageJ to determine fibrosis scoring and quantification of αSMA immunohistochemistry and summarized in Table 2. (b) Total hepatic collagen content in each experimental group analyzed by acidic conversion to hydroxyproline. Box and whiskers plot indicate mean and range (n = 10). (c) Total liver lysates from each experimental group were subjected to western blot analysis of pro-fibrotic SMAD signaling using phosphorylated SMAD2 (p-SMAD2) antibody vs. total SMAD2. Quantitative densitometry analysis is shown as box and whiskers from minimum to maximum values showing all points (d) Fibrogenic gene expression in the livers. mRNA levels were quantified by qPCR. Relative expression levels were normalized against GAPDH. Data presented in bars are means ± SEM (n = 7–9). \*p < .05, \*\*p < .01, \*\*\*p < .001 vs. CD; #p < .05, ###p < .001 vs. NASH PEG; ^p < .05, ^^p < .01, ^^p < .001, vs. NASH OA. (e) Western blot analysis of CTGF and αSMA protein levels in human stellate cells stimulated with TGFβ (20 ng/ml) and increasing concentrations of OA-NO<sub>2</sub> (0.1–2 μM) or OA control (2 μM) for 24 h. (f) Human stellate cells were stimulated with or without TGFβ (20 ng/ml), OA or OA-NO<sub>2</sub> (1 μM). 6 h after TGFβ stimulation fibrogenic gene expression (e.g. ACTA2, CTGF, COL1A1, COL1A2) was analyzed by qPCR. Data shown as mean ± SEM, n = 3. #p < .05, ###p < .001 vs. TGFβ; ^^p < .01, ^^p < .001 vs. TGFβ + OA.

the current study provides a comprehensive landscape of the therapeutic benefits of OA-NO<sub>2</sub> in NASH. Our global transcriptomic analysis identified key pathways involved in lipid metabolism, inflammation and fibrosis, all regulated by OA-NO<sub>2</sub>. Yet, a unifying mechanism could not be identified. Therefore, our study is limited in the mechanistic scope.

NO<sub>2</sub>-FAs are well-established anti-inflammatory agents that regulate the innate immune response [8,11,34]. Indeed, inflammation is centrally involved in the progression of steatohepatitis and fibrosis [35]. Our findings reveal a significant reduction of macrophage infiltration in the liver in response to OA-NO<sub>2</sub> treatment coupled with an attenuated systemic and global hepatic inflammation. Further analysis is

**Table 2**  
Fibrosis score in response to OA-NO<sub>2</sub>.

	Sirius red positive area (%)	αSMA positive area (%)	Fibrosis score
CD	0.22 ± 0.03	0.23 ± 0.04	0.00 ± 0.00
PEG	2.71 ± 0.29 <sup>***</sup>	3.94 ± 0.95 <sup>**</sup>	1.40 ± 0.16 <sup>***</sup>
OA	3.94 ± 0.34 <sup>***</sup>	4.44 ± 0.88 <sup>***</sup>	1.60 ± 0.16 <sup>***</sup>
OA-NO <sub>2</sub>	0.98 ± 0.27 <sup>###,^^</sup>	0.79 ± 0.26 <sup>*,^^</sup>	0.80 ± 0.13 <sup>*,#,,^^</sup>

Fibrosis was scored from 0 to 4 (0: no fibrosis; 1: perisinusoidal or portal fibrosis; 2: perisinusoidal and portal fibrosis; 3: bridging fibrosis; 4: cirrhosis). Data is shown as mean ± SEM

\*\* p < .01.

\*\*\* p < .001 vs. CD.

# p < .05.

### p < .001 vs. NASH PEG.

^^ p < .01.

^^^ p < .001, vs. NASH OA.

required to characterize the contribution of specific liver cells [36–38], including Kupffer cells/macrophages, stellate cells, vascular endothelial cells and hepatocytes in the overall anti-inflammatory role of OA-NO<sub>2</sub> in NASH. Of importance, inhibition of liver fibrosis by OA-NO<sub>2</sub> significantly contributes to the improved liver damage (e.g. reduced plasma levels of ALT and AST). OA-NO<sub>2</sub>-mediated inhibition of fibrogenesis was consistently demonstrated in the liver (e.g. in-vivo imaging, Sirius red-based histology, hydroxyproline content) and in activated stellate cells. Expression of fibrotic genes including CTGF and collagen synthesis were significantly reduced by OA-NO<sub>2</sub>, suggesting that stellate cell activation or myofibroblast conversion in response to TGFβ are attenuated. An analog anti-fibrotic mechanism upon OA-NO<sub>2</sub> treatment operates in other cellular systems [39]. Specifically, preclinical studies on pulmonary fibrosis suggest that OA-NO<sub>2</sub> interferes with TGFβ signaling in lung epithelial cells by mechanisms that involve posttranslational modification of the TGFβ receptor and subsequent receptor dimerization and downstream signaling [35]. Indeed, the expression of TGFβ-mediated pro-fibrotic genes, CTGF and αSMA was significantly attenuated upon OA-NO<sub>2</sub> treatment in HSCs. Our data suggest that OA-NO<sub>2</sub> may modulate, by interfering with TGFβ-induced stellate activation, a reversible phenotypic switch, a process that promotes regression of hepatic pathology during NASH [40,41]. Moreover, TGF-β signaling in hepatocytes contributes to lipid accumulation and NASH development via SMAD signaling [42]. Herein, we show that OA-NO<sub>2</sub> blunted NASH diet-induced SMAD2 activation and over-expression of TGF-β target genes in the NASH liver, indicating the protective effects of OA-NO<sub>2</sub> against both hepatic steatosis and fibrosis via inhibition of the TGFβ/SMAD pathway.

In summary, we provide experimental evidence that OA-NO<sub>2</sub> protects against hepatic steatosis and fibrosis during NASH development. Whereas ongoing phase II clinical trials that include obese patients may provide translational validation of the putative therapeutic benefits of OA-NO<sub>2</sub> against NAFLD, clinical trials specifically designed to test the therapeutic value of OA-NO<sub>2</sub> derivatives for NASH will be critical to pursue.

## Acknowledgements

Not applicable.

## Funding sources

This study was supported by NIH grants R01-HL123333 (LV), R01-HL068878 (YEC), 1R21AI12209801A1 (GX), American Heart Association postdoctoral fellowship 19POST34380224 (OR) and Michigan-Israel Partnership Research Grant (OR, MA). This study utilized services from the University of Michigan In-Vivo Animal Core (IVAC) and the University of Michigan Animal Phenotyping Core, supported by DK020572 (Michigan Diabetes and Research Center), DK089503 (Michigan Nutrition Obesity Research Center), and 1U2CDK110678-01 (Michigan Mouse Metabolic Phenotyping Center).

## Declaration of interests

Xueding Wang declares a pending patent on Photoacoustic physiochemical tissue analysis. All other authors declare no competing interests.

## Author contributions

OR designed and performed experiments, analyzed data, and wrote the manuscript. GX developed, designed and performed all photoacoustic imaging experiments and analyzed the relevant data. YZ assisted with ultrasound imaging and analyzed the relevant data. YG, HW, WL, HL assisted with tissue processing. YL performed in vitro studies. JZ contributed to the experimental design and data interpretation. YF contributed to the discussion. MA contributed to the original concept. ZL, WL contributed to the RNA-sequencing data, bioinformatics analysis, and interpretation. SK contributed to pathway analysis. XW developed photoacoustic ultrasound imaging. YEC contributed to the discussion and interpretation of the data. LV conceived the study, designed, coordinated and performed experiments, analyzed data, and wrote the manuscript.

## Appendix A. Supplementary data

Supplementary data to this article can be found online at <https://doi.org/10.1016/j.ebiom.2019.02.019>.

## References

- Haas JT, Francque S, Staelens B. Pathophysiology and mechanisms of nonalcoholic fatty liver disease. *Annu Rev Physiol* 2016;78:181–205.
- Cohen JC, Horton JD, Hobbs HH. Human fatty liver disease: old questions and new insights. *Science* 2011;332(6037):1519–23.
- Younossi Z, Anstee QM, Marietti M, Hardy T, Henry L, Eslam M, et al. Global burden of NAFLD and NASH: trends, predictions, risk factors and prevention. *Nat Rev Gastroenterol Hepatol* 2018;15(1):11–20.
- Younossi ZM, Koenig AB, Abdelatif D, Fazel Y, Henry L, Wymer M. Global epidemiology of nonalcoholic fatty liver disease—meta-analytic assessment of prevalence, incidence, and outcomes. *Hepatology* 2016;64(1):73–84.
- Rinella ME, Sanyal AJ. Management of NAFLD: a stage-based approach. *Nat Rev Gastroenterol Hepatol* 2016;13(4):196–205.
- Brunt EM, Wong VW, Nobili V, Day CP, Sookoian S, Maher JJ, et al. Nonalcoholic fatty liver disease. *Nat Rev Dis Primers* 2015;1:15080.
- Konerman MA, Jones JC, Harrison SA. Pharmacotherapy for NASH: current and emerging. *J Hepatol* 2018;68(2):362–75.
- Freeman BA, O'Donnell VB, Schopfer FJ. The discovery of nitro-fatty acids as products of metabolic and inflammatory reactions and mediators of adaptive cell signaling. *Nitric Oxide* 2018;77:106–11.
- Rom O, Khoo NKH, Chen YE, Villacorta L. Inflammatory signaling and metabolic regulation by nitro-fatty acids. *Nitric Oxide* 2018;78:140–5.
- Turell L, Steglich M, Alvarez B. The chemical foundations of nitroalkene fatty acid signaling through addition reactions with thiols. *Nitric Oxide* 2018;78:161–9.
- Villacorta L, Minarrieta L, Salvatore SR, Khoo NK, Rom O, Gao Z, et al. In situ generation, metabolism and immunomodulatory signaling actions of nitro-conjugated linoleic acid in a murine model of inflammation. *Redox Biol* 2018;15:522–31.
- Villacorta L, Chang L, Salvatore SR, Ichikawa T, Zhang J, Petrovic-Djergovic D, et al. Electrophilic nitro-fatty acids inhibit vascular inflammation by disrupting LPS-dependent TLR4 signalling in lipid rafts. *Cardiovasc Res* 2013;98(1):116–24.
- Wang H, Liu H, Jia Z, Olsen C, Litwin S, Guan G, et al. Nitro-oleic acid protects against endotoxin-induced endotoxemia and multiorgan injury in mice. *Am J Physiol Ren Physiol* 2010;298(3):F754–62.
- Borniquel S, Jansson EA, Cole MP, Freeman BA, Lundberg JO. Nitrated oleic acid up-regulates PPARgamma and attenuates experimental inflammatory bowel disease. *Free Radic Biol Med* 2010;48(4):499–505.
- Rudolph TK, Rudolph V, Edreira MM, Cole MP, Bonacci G, Schopfer FJ, et al. Nitro-fatty acids reduce atherosclerosis in apolipoprotein E-deficient mice. *Arterioscler Thromb Vasc Biol* 2010;30(5):938–45.
- Zhang J, Villacorta L, Chang L, Fan Z, Hamblin M, Zhu T, et al. Nitro-oleic acid inhibits angiotensin II-induced hypertension. *Circ Res* 2010;107(4):540–8.
- Klinke A, Moller A, Pekarova M, Ravekes T, Friedrichs K, Berlin M, et al. Protective effects of 10-nitro-oleic acid in a hypoxia-induced murine model of pulmonary hypertension. *Am J Respir Cell Mol Biol* 2014;51(1):155–62.
- Rudolph TK, Ravekes T, Klinke A, Friedrichs K, Mollenhauer M, Pekarova M, et al. Nitrated fatty acids suppress angiotensin II-mediated fibrotic remodelling and atrial fibrillation. *Cardiovasc Res* 2016;109(1):174–84.
- Ambrozova G, Martiskova H, Koudelka A, Ravekes T, Rudolph TK, Klinke A, et al. Nitro-oleic acid modulates classical and regulatory activation of macrophages and their involvement in pro-fibrotic responses. *Free Radic Biol Med* 2016;90:252–60.
- Yuan J, Xu G, Yu Y, Zhou Y, Carson PL, Wang X, et al. Real-time photoacoustic and ultrasound dual-modality imaging system facilitated with graphics processing unit and code parallel optimization. *J Biomed Opt* 2013;18(8):86001.
- Bedossa P, Poitou C, Veyrie N, Bouillot JL, Basdevant A, Paradis V, et al. Histopathological algorithm and scoring system for evaluation of liver lesions in morbidly obese patients. *Hepatology* 2012;56(5):1751–9.
- Xu G, Meng ZX, Lin JD, Deng CX, Carson PL, Fowlkes JB, et al. High resolution Physiochemical tissue analysis: towards non-invasive. *In Vivo Biopsy Sci Rep* 2016;6:16937.
- Trajcevski KE, O'Neill HM, Wang DC, Thomas MM, Al-Sajee D, Steinberg GR, et al. Enhanced lipid oxidation and maintenance of muscle insulin sensitivity despite glucose intolerance in a diet-induced obesity mouse model. *PLoS One* 2013;8(8):e71747.
- Pang J, Xi C, Huang X, Cui J, Gong H, Zhang T. Effects of excess energy intake on glucose and lipid metabolism in C57BL/6 mice. *PLoS One* 2016;11(1):e0146675.
- Younossi ZM, Loomba R, Anstee QM, Rinella ME, Bugianesi E, Marchesini G, et al. Diagnostic modalities for nonalcoholic fatty liver disease, nonalcoholic steatohepatitis, and associated fibrosis. *Hepatology* 2018;68(1):349–60.
- Castera L, Friedrich-Rust M, Loomba R. Non-invasive assessment of liver disease in patients with NAFLD. *Gastroenterology* 2019. <https://doi.org/10.1053/j.gastro.2018.12.036>.
- Hui ST, Kurt Z, Tuominen I, Norheim F, Davis RC, Pan C, et al. The genetic architecture of diet-induced hepatic fibrosis in mice. *Hepatology* 2018;68(6):2182–96.
- Schuppan D, Surabattula R, Wang XY. Determinants of fibrosis progression and regression in NASH. *J Hepatol* 2018;68(2):238–50.
- Friedman SL, Neuschwander-Tetri BA, Rinella M, Sanyal AJ. Mechanisms of NAFLD development and therapeutic strategies. *Nat Med* 2018;24(7):908–22.
- Fazzari M, Khoo NK, Woodcock SR, Jorkasky DK, Li L, Schopfer FJ, et al. Nitro-fatty acid pharmacokinetics in the adipose tissue compartment. *J Lipid Res* 2017;58(2):375–85.
- Delmastro-Greenwood M, Freeman BA, Wendell SG. Redox-dependent anti-inflammatory signaling actions of unsaturated fatty acids. *Annu Rev Physiol* 2014;76:79–105.
- Krenkel O, Puengel T, Govaere O, Abdallah AT, Mossanen JC, Kohlhepp M, et al. Therapeutic inhibition of inflammatory monocyte recruitment reduces steatohepatitis and liver fibrosis. *Hepatology* 2018;67(4):1270–83.
- Schopfer FJ, Vitturi DA, Jorkasky DK, Freeman BA. Nitro-fatty acids: new drug candidates for chronic inflammatory and fibrotic diseases. *Nitric Oxide* 2018;79:31–7.
- Hansen AL, Buchan GJ, Ruhl M, Mukai K, Salvatore SR, Ogawa E, et al. Nitro-fatty acids are formed in response to virus infection and are potent inhibitors of STING palmitoylation and signaling. *Proc Natl Acad Sci U S A* 2018;115(33):E7768–E7775.
- Seki E, De Minicis S, Osterreicher CH, Kluwe J, Osawa Y, Brenner DA, et al. TLR4 enhances TGF-beta signaling and hepatic fibrosis. *Nat Med* 2007;13(11):1324–32.
- Cho CS, Park HW, Ho A, Semple IA, Kim B, Jang I, et al. Lipotoxicity induces hepatic protein inclusions through TANK binding kinase 1-mediated p62/sequestosome 1 phosphorylation. *Hepatology* 2018;68(4):1331–46.
- Endo-Umeda K, Nakashima H, Komine-Aizawa S, Umeda N, Seki S, Makishima M. Liver X receptors regulate hepatic F4/80 (+) CD11b(+) Kupffer cells/macrophages and innate immune responses in mice. *Sci Rep* 2018;8(1):9281.
- Kazankov K, Jorgensen SMD, Thomsen KL, Moller HJ, Vilstrup H, George J, et al. The role of macrophages in nonalcoholic fatty liver disease and nonalcoholic steatohepatitis. *Nat Rev Gastroenterol Hepatol* 2018. <https://doi.org/10.1038/s41575-018-0082-x>.

- [39] Reddy AT, Lakshmi SP, Zhang Y, Reddy RC. Nitrated fatty acids reverse pulmonary fibrosis by dedifferentiating myofibroblasts and promoting collagen uptake by alveolar macrophages. *FASEB J* 2014;28(12):5299–310.
- [40] Kisseleva T, Cong M, Paik Y, Scholten D, Jiang C, Benner C, et al. Myofibroblasts revert to an inactive phenotype during regression of liver fibrosis. *Proc Natl Acad Sci U S A* 2012;109(24):9448–53.
- [41] Jun JI, Lau LF. Resolution of organ fibrosis. *J Clin Invest* 2018;128(1):97–107.
- [42] Yang L, Roh YS, Song J, Zhang B, Liu C, Loomba R, et al. Transforming growth factor beta signaling in hepatocytes participates in steatohepatitis through regulation of cell death and lipid metabolism in mice. *Hepatology* 2014;59(2):483–95.